3196

Sub 2 mm resolution fMRI at 3T using randomly undersampled 3D-EPI with locally low-rank + temporally sparse reconstruction

Rex T.L. Fung[1,2], Rodrigo A. Lobos[2], Jeffrey A. Fessler[2,3,4], Douglas C. Noll[1,2,4], and Jon-Fredrik Nielsen[1,2,4]
[1]*Functional MRI Laboratory, University of Michigan, Ann Arbor, MI, United States,* [2]*Biomedical Engineering, University of Michigan, Ann Arbor, MI, United States,* [3]*Electrical and Computer Engineering, University of Michigan, Ann Arbor, MI, United States,* [4]*Radiology, University of Michigan, Ann Arbor, MI, United States*

Synopsis

Keywords: New Trajectories & Spatial Encoding Methods, New Trajectories & Spatial Encoding Methods, Sparse & Low-Rank Models

Motivation: Many fMRI applications require sub 2 mm resolution, but most existing methods lose functional sensitivity at sub 2 mm resolution due to thermal noise, especially at 3T.

Goal(s): To investigate and develop acquisition and reconstruction methods for high resolution BOLD fMRI at 3T.

Approach: 3D-EPI with randomized sampling was used for acquisition. Images were reconstructed via locally low-rank plus sparse decomposition. A finger tapping task is used for testing.

Results: Motor activation was detected at 1.8 mm resolution, with our protocol producing activation maps with higher specificity compared to standard reconstruction methods.

Impact: Randomized 3D-EPI and locally low-rank plus temporally sparse decomposition are novel approaches for high resolution fMRI. Other fMRI scientists can use our vendor-agnostic, open-source implementation as a template, adapting it to suit their specific high resolution fMRI needs.

Introduction

Typical 3T fMRI protocols use SMS-EPI with 2.4 mm spatial resolution and 0.8 s volume TR [1][2]. This is insufficient for higher resolution applications such as brainstem, hippocampal, or layer-specific fMRI [3][4][5]. Increasing spatial resolution means lower SNR and longer encoding times, and to combat that, low rank spatial and/or temporal modeling has been proposed, both as a denoising step and as image reconstruction regularization. However, how to best implement such methods to detect functional signal while achieving reduced noise and aliasing artifacts is an open research question. Here we report an open-source, vendor-neutral implementation of a randomized 3D-EPI acquisition and locally low-rank plus temporally sparse (LLR + S) reconstruction pipeline. We demonstrate our protocol's feasibility through an fMRI experiment at 1.8 mm resolution.

Methods

Compressed sensing approaches to MRI [6] says that randomly sampling k-space results in incoherent aliasing artifacts that are easier to remove, so we investigated 3D-EPI with random undersampling along ky and kz. We generated sampling patterns independently for each time point, which should improve the spatial and temporal incoherence of aliases. Given that SNR generally increases towards the center of k-space, we sampled each location with a probability depending on its distance from the origin based on a zero-mean Gaussian distribution, while also enforcing a fully sampled central region. For every echo train, we fixed both the echo train length and the number of echoes before crossing ky = 0 to achieve a consistent TE of 30 ms for T2* contrast, and constrained the gaps between consecutive echoes to prevent the need for large gradient blips.

For reconstruction, we try to minimize:

$$\underset{L,S}{\arg\min}\ \frac{1}{2}\|\mathbf{E}(L+S)-d\|_2^2+\lambda_L\sum_{p=1}^{N_p}\|\mathbf{P}_p(L)\|_*+\lambda_S\|\mathbf{T}S\|_1$$

where:

- $X = L + S, X \in \mathbb{C}^{N_s \times N_t}$ denotes the underlying image matrix to be reconstructed. $N_s = N_x N_y N_z$ denotes number of spatial locations.
- $L, S \in \mathbb{C}^{N_s \times N_t}$ denotes the LLR and S component matrices.
- $d \in \mathbb{C}^{N_s N_t N_c / R}$ denotes the measured k-space vector. N_c denotes number of receiver coils. R denotes acceleration factor.
- $\mathbf{E} : \mathbb{C}^{N_s \times N_t} \to \mathbb{C}^{N_s N_t N_c / R}$ denotes MRI forward operator, mapping the image to k-space.
- $\mathbf{P}_p : \mathbb{C}^{N_s \times N_t} \to \mathbb{C}^{N_{x,patch} N_{y,patch} N_{z,patch} \times N_t}$ denotes the pth patch extraction operator. N_p denotes number of patches.
- $\mathbf{T} : \mathbb{C}^{N_s \times N_t} \to \mathbb{C}^{N_s \times N_t}$ denotes the unitary temporal FT operator.
- λ_L, λ_S denote regularization parameters.

Figure 3 illustrates the iterative algorithm for LLR + S image reconstruction. For patch extraction, overlapping cubic patches with fixed size and stride were used. Patch sizes were chosen such that $N_{x,patch} N_{y,patch} N_{z,patch} \approx N_t$ for singular value decomposition efficiency. Strides varied from 1 to 4, trading between reconstruction quality and speed.

For experimental validation, we used a finger tapping task with alternating 20 second blocks of tap/rest for 7 cycles. T2*-weighted images were acquired using 3D-EPI with the following parameters: FOV = $21.6 \times 21.6 \times 7.2$ (in cm), resolution = 1.8 mm^3, acquisition array = $120 \times 120 \times 40$, volume TR = 0.9 s, acceleration factors = [R_y, R_z] = [2, 2.86].

Results & Discussion

Figure 4 shows that LLR + S reconstruction detects motor activation with similar sensitivity as SENSE reconstruction with ℓ_1-regularization in the spatial wavelet domain. LLR + S images show fewer false activations outside the brain, which we speculate is due to removal of temporally incoherent aliasing artifacts during promotion of low-rankness. Residual aliasing artifacts in the S/I (z) direction are observed, as expected from our sampling pattern design.

Conclusion

Our randomized 3D-EPI and LLR + S protocol produced feasible activation maps at 1.8 mm. Randomized ky and kz undersampling results in spatially and temporally incoherent aliases, which are removed along with noise by LLR + S reconstruction. Other fMRI scientists can use our vendor-agnostic, open-source implementation as a template, adapting it to suit their specific high resolution fMRI needs to study new regions such as the brainstem, hippocampus, and specific cortical layers.

Several future research directions follow our work. First, a tailored RF pulse can be used with 3D-EPI to image an even smaller, non-cuboid volume. Second, sampling trajectory can be further improved, such as sampling multiple kz locations in one shot to increase incoherence of aliases. Third, theory for tuning LLR reconstruction parameters for specific imaging applications have yet to be established and should be valuable given the recent popularity of LLR models.

Acknowledgements

This work was supported by NIH grant U24-NS120056.

We would like to thank David Frey for helping with calculating and visualizing t-scores for functional analysis.

References

1] Betty Jo Casey et al. "The adolescent brain cognitive development (ABCD) study: imaging acquisition across 21 sites". In: *Developmental cognitive neuroscience* 32 (2018), pp. 43–54.

[2] Kawin Setsompop et al. "Blipped-controlled aliasing in parallel imaging for simultaneous multislice echo planar imaging with reduced g-factor penalty". In: *Magnetic resonance in medicine* 67.5 (2012),pp. 1210–1224.

[3] F Beissner. "Functional MRI of the brainstem: common problems and their solutions". In: *Clinical neuroradiology* 25.Suppl 2 (2015), pp. 251–257.

[4] Nanthia A Suthana et al. "High-resolution 7T fMRI of human hippocampal subfields during associative learning". In: *Journal of cognitive neuroscience* 27.6 (2015), pp. 1194–1206.

[5] Peter A Bandettini, Laurentius Huber, and Emily S Finn. "Challenges and opportunities of mesoscopic brain mapping with fMRI". In: *Current Opinion in Behavioral Sciences* 40 (2021), pp. 189–200.

[6] Michael Lustig, David Donoho, and John M Pauly. "Sparse MRI: The application of compressed sensing for rapid MR imaging". In: *Magnetic Resonance in medicine* 58.6 (2007), pp. 1182–1195.

[7] Rüdiger Stirnberg et al. "Rapid whole-brain resting-state fMRI at 3 T: Efficiency-optimized three-dimensional EPI versus repetition time-matched simultaneous-multi-slice EPI". In: Neuroimage 163 (2017), pp. 81–92.

[8] Ricardo Otazo, Emmanuel Candes, and Daniel K Sodickson. "Low-rank plus sparse matrix decomposition for accelerated dynamic MRI with separation of background and dynamic components". In: *Magnetic resonance in medicine* 73.3 (2015), pp. 1125–1136.

[9] Kelvin J Layton et al. "Pulseq: a rapid and hardware-independent pulse sequence prototyping framework". In: *Magnetic resonance in medicine* 77.4 (2017), pp. 1544–1552.

[10] Jon-Fredrik Nielsen and Douglas C Noll. "TOPPE: A framework for rapid prototyping of MR pulse sequences". In: *Magnetic resonance in medicine* 79.6 (2018), pp. 3128–3134.

[11] Rodrigo A Lobos, Chin-Cheng Chan, and Justin P Haldar. "New theory and faster computations for subspace-based sensitivity map estimation in multichannel MRI". In: *IEEE Transactions on Medical Imaging* (2023).

[12] Jeffrey A Fessler. Michigan Image Reconstruction Toolbox (Julia version). URL: https://github.com/JeffFessler/MIRT.jl.

[13] Martin Uecker et al. "The BART toolbox for computational magnetic resonance imaging". In: *Proc Intl Soc Magn Reson Med*. Vol. 24. 2016, p. 1.

Figures

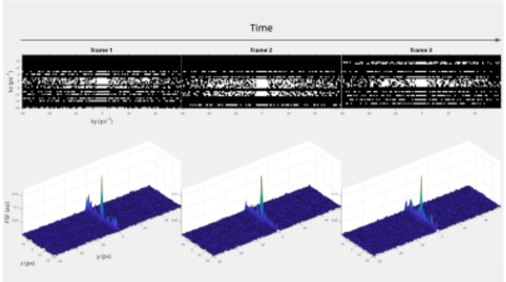

Randomized ky and kz sampling results in spatially incoherent aliasing artifacts along y and z. Top row: sampling masks (every point represents a fully sampled kx line). Bottom row: corresponding point spread functions in the image domain, where height and color represent intensity. Aliasing along z is still quite coherent as kz locations are still being sampled in an all-or-none fashion. Changing sampling along time results in temporally incoherent aliasing artifacts.

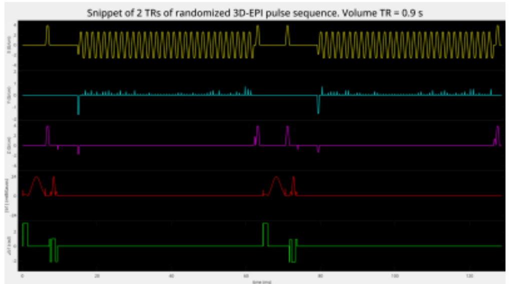

Snippet of pulse sequence consisting of 2 TRs. Each excitation acquires a kx-ky plane at one kz location. Number of excitations per volume corresponds to number of kz locations to be sampled. Fat saturation is applied every TR. Echo spacing, defined as the time interval between consecutive echoes, is fixed for effective pulse sequence storage, which may result in complicated off-resonance artifacts.

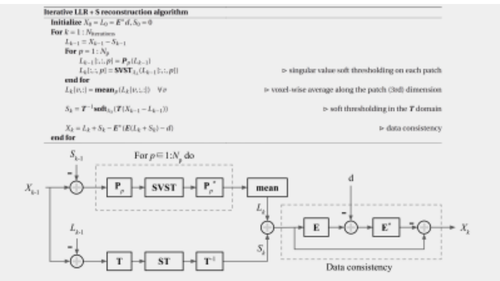

Iterative algorithm for LLR + S image reconstruction. Bottom: sequence of operations for the kth iteration. First, singular value soft-thresholding (SVST) is applied to patches $L_{k-1} = X_{k-1} - S_{k-1}$ then recombined to get L_k. Here, overlapping patches are used to avoid blocky artifacts. Mean denotes voxel-wise averaging across all contributing patches. Second, soft-thresholding (ST) is applied in the temporal Fourier Transform of $S_{k-1} = X_{k-1} - L_{k-1}$ to get S_k. Third, data consistency is enforced to get X_k.

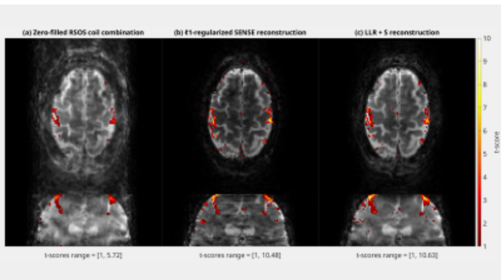

(c) LLR + S reconstruction detects motor activation at 1.8 mm resolution with similar sensitivity to (b) ℓ_1-regularized SENSE reconstruction with significantly fewer false detections outside the brain. (a) zero-filled root-sum-of-squares (RSOS) combined images show aliasing artifacts that are removed by both reconstruction methods, although motor activation can still be detected at lower significance. Activation (t-score) maps are thresholded at 1, then overlaid onto the 1st frame of T2*-weighted images.

Proc. Intl. Soc. Mag. Reson. Med. 33 (2025)
3196